40

MODELING OF SAR SIGNATURES OF SHALLOW WATER OCEAN TOPOGRAPHY

R.A. Shuchman, A. Kozma, E.S. Kasischke, and D.R. Lyzenga
Radar Division
Environmental Research Institute of Michigan
P.O. Box 8618
Ann Arbor, Michigan 48130

ABSTRACT

A hydrodynamic/electromagnetic model has been developed for the purpose of explaining and quantifying the relationship between the Seasat synthetic aperture radar (SAR) observed signatures and the bottom topography of the ocean in the English Channel region of the North Sea. The model uses environmental data (wind, current and water depth changes), and radar system parameters (frequency, polarization, incidence angle and resolution cell size) as inputs and predicts SAR-observed backscatter changes over topographic changes in the ocean floor. The model results compare quite favorably with the actual Seasat SAR-observed backscatter values. The comparisons between the model and the actual data are all within 1.5 dB. The developed model is valid for only relatively shallow water areas (i.e., less than 50 meters in depth) and suggests that for bottom features to be visible on SAR imagery, a moderate to high velocity current (0.40 m/s or greater) and a moderate wind (between 1 and 7.5 m/sec) must be present.

1. INTRODUCTION

The Seasat synthetic aperture radar (SAR) launched in 1978 by NASA, collected ocean imagery during approximately 200 of the 1500 orbits it was in operation. Although this SAR system operated at L-band (23.5 cm), a wavelength which does not penetrate an appreciable distance into the water, the data from Seasat revealed many patterns that are apparently related to subsurface or bottom features. An extensive study reported by Kasischke, et al. (1983 and 1983a) examined all passes of Seasat SAR imagery collected over non-frozen ocean regions for evidence of bottom-related surface signatures. In this study, the positions of the unidentified patterns which were suspected to be bottom-induced were determined by identifying known land areas or through the use of satellite ephemeris records. Hydrographic charts from these areas were examined to determine whether or not the patterns occurred over a distinct bottom feature.

Of the some 200 orbits of Seasat-SAR imagery examined, approximately 80 percent were found to contain patterns on the imagery which could be correlated to a distinct bottom feature. Kasischke, et al. (1983) reports on 35 test cases which were rigorously examined and the surface patterns on the imagery compared with hydrographic charts and ancillary data (environmental conditions coincident with the satellite overpass). These test cases are presented in Table 1.

The probable cause for observation of many of these features is that they induce local changes in the ocean surface currents which in turn cause changes in the small scale wave structure on the ocean surface. The observed SAR backscatter is a function of this small scale, or Bragg roughness (Wright, 1966 and Vesecky and Stewart, 1982). Many of the subsurface features observed by Seasat have been explained through the use of hydrodynamic/electromagnetic numerical modeling efforts.

TABLE 1
SUMMARY OF SEASAT SAR IMAGERY EXAMINED FROM BATHYMETRIC FEATURES
(modified from Kasischke, et al., 1983)

Study Site (Location)	Seasat Revolution	Date	Time (GMT)	Bottom Feature(s)*
Little Bahama Bank -- Grand Bahama Island	407	25 July 1978	12:46	EB
	651	11 August 1978	12:26	EB
Great Bahama Bank -- Bimini	407	25 July 1978	12:46	EB
	651	11 August 1978	12:26	EB
Great Bahama Bank -- Southern Edge	407	25 July 1978	12:46	EB
	651	11 August 1978	12:26	EB
Tongue of the Ocean	450	28 July 1978	06:23	EB, SWS
	529	02 August 1978	18:37	EB, SWS
	694	14 August 1978	07:37	EB, SWS
	1024	06 September 1978	09:18	EB, SWS
	1110	12 September 1978	09:43	EB, SWS
	1153	15 September 1978	09:56	EB, SWS
	1196	18 September 1978	10:09	EB, SWS
	1239	21 September 1978	10:21	EB, SWS
	1282	24 September 1978	10:34	EB, SWS
	1325	27 September 1978	10:47	EB, SWS
	1368	30 September 1978	11:00	EB, SWS
	1411	03 October 1978	11:12	EB, SWS
Haiti -- Rochelois Bank	432	31 July 1978	11:28	SI
Bermuda	1267	23 September 1978	14:20	SI
Nantucket Shoals	880	27 August 1978	12:25	SWS
Cook Inlet, Alaska	289	17 July 1978	11:50	SWS, MB
North Rona Rock	762	19 August 1978	06:41	SI
Sula Sgier	762	19 August 1978	06:41	SI
English Channel	762	19 August 1978	06:41	SWS, MB
	957	01 September 1978	21:40	SWS
	1430	04 October 1978	20:42	SWS
	1473	08 October 1978	00:15	SWS
Northeast Atlantic	547	04 August 1978	06:15	DWB, DWR, DWS, DWSM
	556	04 August 1978	21:35	DWB, DWR, DWS, DWSM
	599	07 August 1978	21:43	DWB, DWR, DWS, DWSM
	633	10 August 1978	06:29	DWB, DWR, DWS
	642	10 August 1978	21:50	DWR, DWS, DWSM
	719	16 August 1978	06:43	DWB, DWR, DWS
	757	18 August 1978	22:40	DWB, DWR, DWS
	762	19 August 1978	06:41	DWB, DWR, DWS
	791	21 August 1978	07:24	DWB, DWR, DWS, DWSM
	834	24 August 1978	07:30	DWB, DWR, DWS
	958	01 September 1978	23:54	DWB, DWR
	1006	05 September 1978	08:15	DWB, DWR, DWS
	1044	08 September 1978	00:18	DWB, DWR
	1049	08 September 1978	08:27	DWB, DWR, DWS
	1087	11 September 1978	00:30	DWB, DWR

*Bottom Feature Key:

DWB	Deep Water Bank
DWR	Deep Water Ridge
DWS	Deep Water Shelf
DWSM	Deep Water Seamount
EB	Edge of Bank in the Carribean
MB	Mud Bank
SL	Shoal area surrounding an island
SWS	Shallow Water Sand Bank

One of the most dramatic and least expected results obtained from Seasat was the observation of very distinct patterns related to transverse sand waves and longitudinal sand bars. These features are summarized by the SWS symbol on Table 1. These SAR-observed features correspond very well to the local bottom bathymetric features and have been noted on SAR data of ocean regions of up to 50 meters in depth. Examination of environmental data (winds, gravity waves, air/sea temperature, density stratification and currents) indicates the SAR observed features are only present when a tidal current (0.4 m/s or greater) is flowing over the bottom and a minimum wind (~1 m/s) with a favorable direction is present. This minimum wind is necessary to generate ocean Bragg waves which reflect the radar's incident electromagnetic waves. It is hypothesized that the refraction, straining, and in some cases, blocking of these Bragg waves by the currents is responsible for the observed bottom features.

One of the most vivid of these shallow water sand banks (SWS) expressions examined in the Seasat study are those associated with shoal regions of the Southern Bight of the North Sea (English Channel). This region is characterized by shallow (less than 50 meter water depth), subaqueous banks and sand waves, and it is this test site that was utilized in this study.

This paper first presents a theory for SAR detection of ocean surface patterns. This SAR imaging mechanism is then utilized along with a hydrodynamic theory to describe the observation of subsurface features on the Seasat SAR English Channel data set. The hydrodynamic/electromagnetic theory is then combined into a numerical model whose results are compared to the actual Seasat SAR data.

2. SAR IMAGING MECHANISMS

The patterns observed on SAR images of the ocean surface are the result of a complex set of imaging mechanisms including real modulations and effects due to the motion of the surface. In addition, the detectability of any given surface pattern is influenced by the variability of the background signal, which is due to speckle as well as random surface fluctuations.

Real modulations consist of variations in the small-scale and large scale roughness, where the length scale depends on the radar wavelength. Small-scale roughness influences the radar return through the Bragg scattering mechanism, and possibly also through "wedge scattering" from cusped waves (Lyzenga, et al., 1983). There is a general concensus within the radio-oceanography community that a Bragg-Rice scattering theory can explain to a large degree the SAR-observed backscatter values obtained from the ocean surface at intermediate incidence angles (20-60°). That is, the transmitted radar energy with wave number k_o interacts in a resonant or interference fashion with ocean surface waves with wave number k_w such that

$$k_w = 2k_o \sin \theta, \tag{1}$$

where $k_w = 2\pi/L$ and $k_o = 2\pi/\lambda$, L and λ are the wavelengths of the surface waves and the radar respectively, and θ is the incidence angle. Large-scale roughness perturbations cause a change in the Bragg scattering due to a local tilting of the surface as well as changes in the amount of specular reflection. For the case of internal waves and bottom topographic features, the real modulations are result

of interactions between wind-generated surface waves and the surface currents induced by the subsurface phenomena of interest. This real modulation represents what a "real aperture" imaging radar or scatterometer would observe.

Motion effects are also a primary contributor to SAR images of the ocean surface. Recall SAR, to achieve its high resolution, observes the ocean for a period of time (the integration time) to generate the synthetic antenna. A moving ocean surface results in a perturbation of the phase of the scatterers during this time interval and this results in an altered image (Jain, 1978; Alpers and Rufenach, 1979; and Shuchman, et al., 1981). Ordered motions of the sea surface, such as orbital velocities and accelerations due to gravity and internal waves, can cause velocity bunching (i.e., periodic regions of increased and decreased image intensity) in the images (Alpers, et al., 1981) Scatterer accelerations degrade the resolution of the images in a predictable way (Lyzenga and Shuchman, 1983). A second category of motions which are random in nature also contribute to the SAR signatures of the ocean. Random motions cause azimuth smearing or streaking of the images. Random motions on a scale smaller than the SAR resolution may be described in terms of the coherence time or lifetime of the ocean scatterers.

The third factor which contributes to the detectability of SAR-observed signatures is the background signal variability. This variability is due to both speckle and large-scale surface variations which are unrelated to the phenomenon of interest. Speckle is a result of the coherent nature of the SAR system (Harger, 1970). Scatterers which are randomly distributed within each pixel interfere either constructively or destructively to create the "salt and pepper" images characteristic of a SAR. The speckle size is a function of the spatial resolution. The speckle intensity can be reduced by utilizing multi-look processing (or noncoherent addition) techniques during processing of the SAR signals.

Random surface variations also contribute to the background variability in SAR ocean surface images. These large-scale variations can be a result of a number of oceanographic phenomena including gravity waves, either well organized or random in nature, variable wind creating patchiness on the ocean surface, rain squalls, and mesoscale features such as ocean fronts (Shuchman, 1982).

3. DATA DESCRIPTION

Four Seasat revolutions provide SAR coverage of the Southern Bight region of the North Sea and English Channel. The SAR swaths (100 km wide) are indicated as rectangles on Figure 1. The SAR passes used in the study are Revolutions 762, 957, 1430, and 1473. As indicated on Table 2 (a summary of SAR data collected over the test site), the satellite overpasses span the time from August 19 to October 8, 1978, representing late summer conditions in the Channel. Note from Table 2 and Figure 1 that Revolutions 957, 1430, and 1473 have generally the same orientation (i.e., radar look direction with respect to the Channel), while Revolution 762 represents the nearly orthogonal look direction. The English Channel test site is characterized by a series of longitudinal and transverse sand waves which are situated in water depth varying from approximately 50 to 3 meters (Kenyon, et al., 1979). Table 3 summarizes the environmental conditions present in the English Channel at the time of the four Seasat passes.

Figure 2 is a detailed comparison of the radar image and the bathymetric chart of the bottom in the test area for Revolution 762. From Figure 2, it can be noted

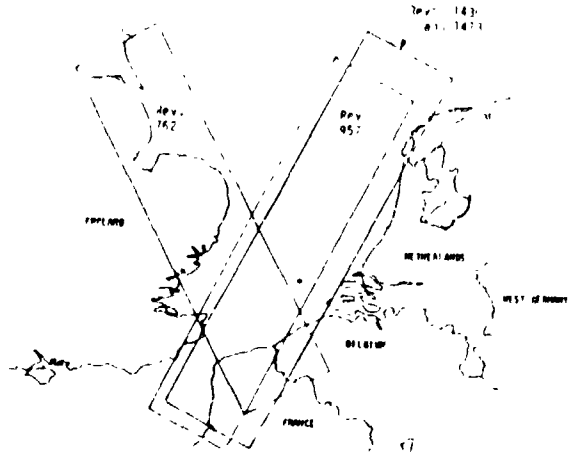

FIGURE 1. GROUND COVERAGE OF SEASAT REVOLUTIONS USED FOR ENGLISH CHANNEL ANALYSIS

TABLE 2
SAR SYSTEM AND SATELLITE PARAMETERS FOR STUDY SITES

Revolution	Date	Node	Time Over Target Channel (GMT)	Satellite Heading (T°)	SAR Look Direction (T°)	Incident Angle (Degrees) Near-Far
762	8-19-78	25.02	06:30	333°	63°	20°-25.2°
957	9-1-78	172.05	21:40	223°	313°	19.6°-24.9°
1430	10-4-78	172.76	00:40	223°	313°	19.6°-24.9°
1473	10-8-78	172.26	00:15	223°	313°	19.6°-24.9°

TABLE 3
ENVIRONMENT DATA RECORDED AT THE TIME OF SATELLITE OVERPASS

Revolution	Visibility of Subsurface Features	Wind[1] Speed Direction	Water Temp.	Air Temp.	Wave Ht.	Period of Waves	Current[2] Speed and Direction	Current[3] Speed and Direction	A Typical Water Depth at Feature	Fra. de Number[4] Fr = v/√gD	Reynolds[4] Number Re = vD/ν
762	Very Visible	6.0 kn 140°(T)	16.4°(C)	17°(C)	0.5 m	1 s	1.4 kn 210°(T)	1.0 kn 220°(T)	7.6 m	0.08	3.88×10^6
957	Very Faint	20.0 kn 320°(T)	16.5°(C)	15°(C)	1.0 m	4 s	0.2 kn 210°(T)	0.2 kn 270°(T)	12.1 m	0.01	0.77×10^6
1430	Very Faint	21.0 kn 315°(T)	15.5°(C)	11°(C)	1.0 m	4 s	1.3 kn 30°(T)	1.5 kn 40°(T)	13.1 m	0.08	0.17×10^6
1473	Moderately Visible	11.0 kn 15°(T) 200°(T)	15.2°(C)	15°(C)	0.5 m	3 s	1.2 kn 210°(T)	0.7 kn 210°(T) 200°(T)	10.0 m	0.06	0.78×10^6

1 kn = 0.51 m/s

[1]Standard meteorological convention (i.e., direction from).

[2]Direction current is flowing towards (value is near South Falls sand bank).

[3]Average current value for test area.

[4]Values repeated from Table 3 for completeness.

NOTE: In all cases, the water column was unstratified, and no rainfall or ocean swell was present.

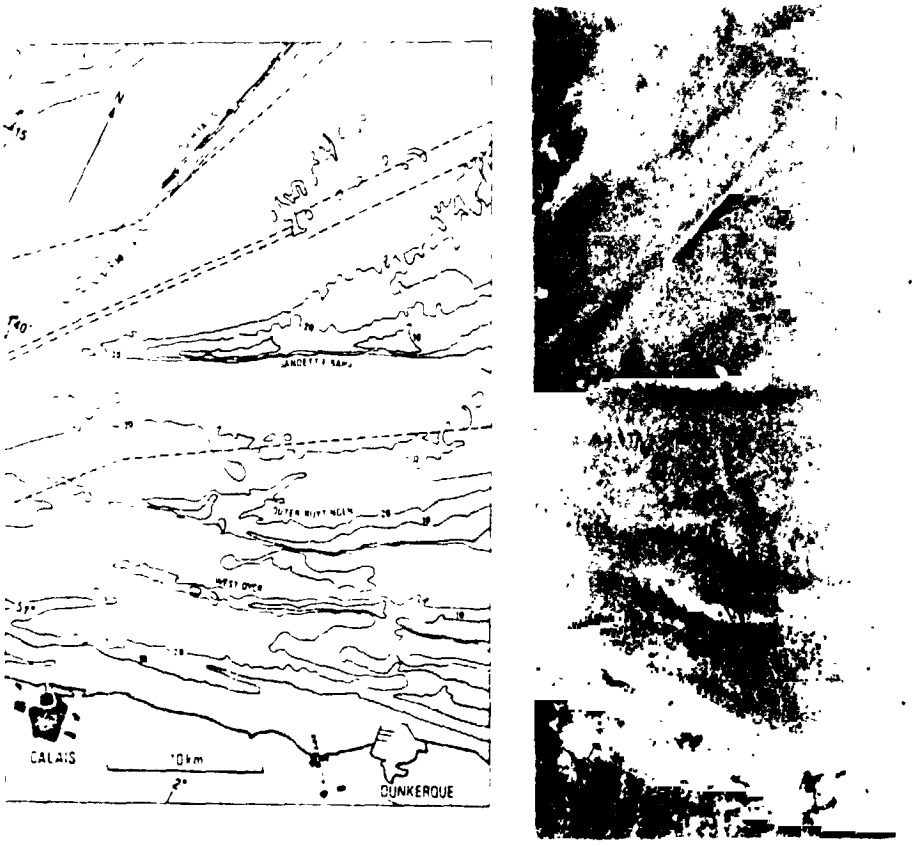

(The dashed lines in the figure are recommended ship routes)

FIGURE 2. COMPARISON OF SAR IMAGE AND CHART OF THE SEA BED EAST OF DOVER STRAITS

that the sand waves are visible with stronger radar returns resulting on the down current side of their crest lines. The transverse sand waves are predominantly on the gentler slope of the asymmetrical longitudinal sand waves (or banks) and their crest lines bend around to trend increasingly more parallel to the longitudinal sand wave axis. Kenyon (1981) reports at the time of this image collection a current of 1-2 m/s was flowing 20° obliquely to the longitudinal sand waves and parallel to the orthogonal of the transverse waves. It is further noted that analysis of sidescan sonar records from near South Falls has revealed additional transverse sand waves which are not seen on the image (Kenyon, 1981 and Caston 1979).

4. MODELING OF BOTTOM DEPTH-RELATED PATTERNS ON SAR IMAGERY

In order to better quantify the relationship between SAR-observed sand ridges and environmental (wind, water depth, current speed, water temperature, etc.) and the SAR system (frequency, polarization, resolution, incident angle, look direction, etc.) parameters necessary to image these features, a hydrodynamic/electromagnetic modeling effort was undertaken.

A flow chart for the hydrodynamic/ electromagnetic model is presented in Figure 3. The model utilizes both environmental and SAR system parameters as inputs. The environmental inputs include: wind speed (m/s) and direction (degrees); initial current velocity (m/s) and direction (degrees); and water depth (m) on a grid basis. The SAR system parameters include: wavelength (cm); polarization (either vertical or horizontal); incidence angle (degrees), radar look angle (degrees), and resolution (m). The model first calculates the Bragg ocean wavelength using a two-scale scattering model where the long waves or slopes are neglected. A current profile is then computed as a function of the irregular topography (changing depth).

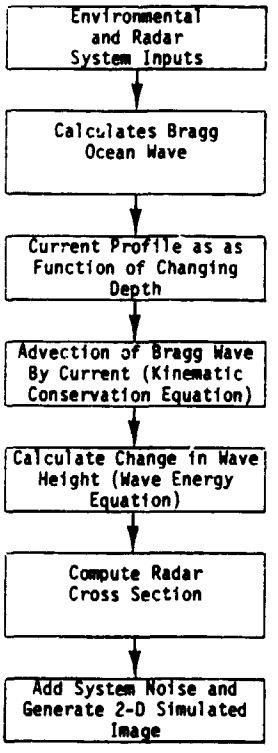

FIGURE 3. FLOW CHART FOR HYDRODYNAMIC/ELECTROMAGNETIC MODEL

The interaction of a tidal current with the bottom is presently described in terms of a simple quasi-one-dimensional model. The model considers a linear ridge of effectively "infinite" length with a parabolic cross section. This is equivalent to assuming that the component of the current parallel to the ridge is constant, i.e., that none of the water is allowed to flow around the shallow feature. Thus, only the perpendicular component varies, and this component can be calculated simply by conservation of mass. Assuming that the vertical current profile is constant, the surface velocity is then given by

$$V_x(X) = V_x(X_0)\,\frac{Z_0}{Z} \qquad (2)$$

$$V_y(X) = V_y(X_0) \qquad (3)$$

where $V_x(X_o)$ and $V_y(X_o)$ are the perpendicular and parallel components of the current outside of the ridge respectively, Z_o is the depth at the location (X_o), and Z is the depth at the location (X) under consideration.

The interaction of surface gravity waves with a variable current has been described by Hughes (1978) and Phillips (1977, 1981), among others. This interaction is described by two equations, the kinematic (or wave) conservation equation, and the wave action (or energy) equation. The former equation may be written as

$$\frac{\partial \vec{k}}{\partial t} + \vec{\nabla}(\omega + \vec{k} \cdot \vec{V}) = 0 \tag{4}$$

where k is the wave number, $\omega = \sqrt{gk}$ is the radian frequency of the wave, and V is the current velocity. In the steady-state case, the first term (i.e., the time derivative) may be ignored. For the one-dimensional case considered in the simple current interaction model, the solution of this equation may be written as

$$\omega + k_x V_x = \omega_o + k_{xo} V_{xo} \tag{5}$$

$$k_y = k_{yo} \tag{6}$$

where k_x and k_y are the wave number components perpendicular and parallel to the ridge, respectively, and k_{xo}, k_{yo} are their values in the constant-current region away from the ridge. These equations express the changes in the wavelength and direction of a wave entering a variable current.

The changes in wave amplitude are described by the wave action equation, which may be written as

$$\frac{\partial \phi}{\partial t} + \left(\vec{V} + \frac{\partial \omega}{\partial \vec{k}}\right) \cdot \vec{\nabla}\phi = \beta\phi\left(1 - \frac{\phi}{\phi_\infty}\right) \tag{7}$$

where $\phi = \psi/\omega$ is the action spectrum, ($\psi(k)$ is the wave height spectrum), β is a wave growth parameter related to the wind speed and direction (Hughes, 1978), and ϕ_∞ is the equilibrium spectrum for the given wind conditions. The solution of this equation for the steady-state one-dimensional problem under consideration may be written in terms of the wave height spectrum as

$$\frac{1}{\psi(k)} = \frac{1}{\psi_\infty(k)} + \frac{1}{\psi_o(k_o)} - \frac{1}{\psi_\infty(k)} \; e^{-\beta(x-x_o)\left(u_x + \frac{\partial \omega}{\partial k_x}\right)^{-1}} \tag{8}$$

where the wave number k is related to the initial wave number k_o (at a location away from the ridge).

As an example, consider the case of a wave field being carried by a current over a ridge in the bottom. As the wave propagates into a region of increasing current (i.e., as it approaches the ridge), it is elongated and the amplitude is decreased. If there is a wind in the same direction ($\beta > 0$), the amplitude

gradually builds back up toward its equilibrium value. After the wave passes the shallowest point, the current then decreases and the waves become shorter and of higher amplitude. Under zero-wind conditions, the amplitude would return to the original value resulting in only a dark band over the ridge. For a wind in the same direction as the current, the wave amplitude would increase beyond the initial value, resulting in regions of both lesser and greater wave height or surface roughness than the "background" value.

The wave height spectra obtained from this model were used to compute changes in the radar cross section of the surface, using a composite scattering model. Noise is then added to the modeled output to simulate speckle in the Seasat data and a two-dimensional image is generated.

Quantitative results from this model were compared with a series of relative radar backscatter measurements made from digital and optical data from the four Seasat SAR English Channel revolutions. The backscatter measurements were made at the output plane of the ERIM optical SAR processor using an optical probe; thus, the effects of recording the radar data on film could be neglected.

In addition to the optical measurement, the digital data for Revolution 762 was also analyzed. The digital data was averaged to obtain backscatter values representing the same area as the optical probe.

Three locations within the English Channel were selected for detailed study (i.e., the generation of modeled results). The English Channel test sites included South Falls and Sandettie Sand Banks (see Figure 2 for location) and a series of transverse sand waves resting in approximately 32 meters of water, the wave crests of which are aligned perpendicularly to Sandettie Bank. The transverse sand waves have a wavelength of approximately 400 meters and amplitude of 6.5 meters with the crests of the sand waves approximately 25 m below the water surface.

Figure 4 shows the optically generated 25 km quarter swath images for the four revolutions of the English Channel and also indicates the location of an optical scan made over the vicinity of South Falls (1A). Note the optical images confirm that the sand features are very visible on Revolution 762 imagery, moderately visible on Revolution 1473 imagery, and not visible (or very faintly visible) on imagery from Revolutions 1430 and 957. Also shown on the figure are the locations of optical scans (2A) made over the Sandettie Bank. The location of the transverse sand wave measurement is indicated as the letter 3A. Recall the SAR system and environment parameters for these four revolutions are summarized in Tables 2 and 3, respectively.

A model-generated reflectivity map of South Falls Revolution 762 is presented in Figure 5. In this figure, the computer-generated gray map represents an area of 2.5 x 2.5 km where each value (pixel) represents 20 x 20 m. As presented on the legend of the figure, each symbol on the gray map represents a 0.5 dB level. Figure 6 represents the idealized cross section of South Falls at the time of satellite overpass which was modeled. The reflectivity map presented in Figure 5 demonstrates the capability of the model to provide a two-dimensional output (i.e., a simulated SAR image).

Table 4 summarizes the modeled versus actual SAR backscatter values. For the modeled and actual SAR backscatter values, the change in the σ_0 value across the bottom feature is given. Both the optically- and digitally-extracted backscatter values are presented in Table 4. These optical and digital values differed by

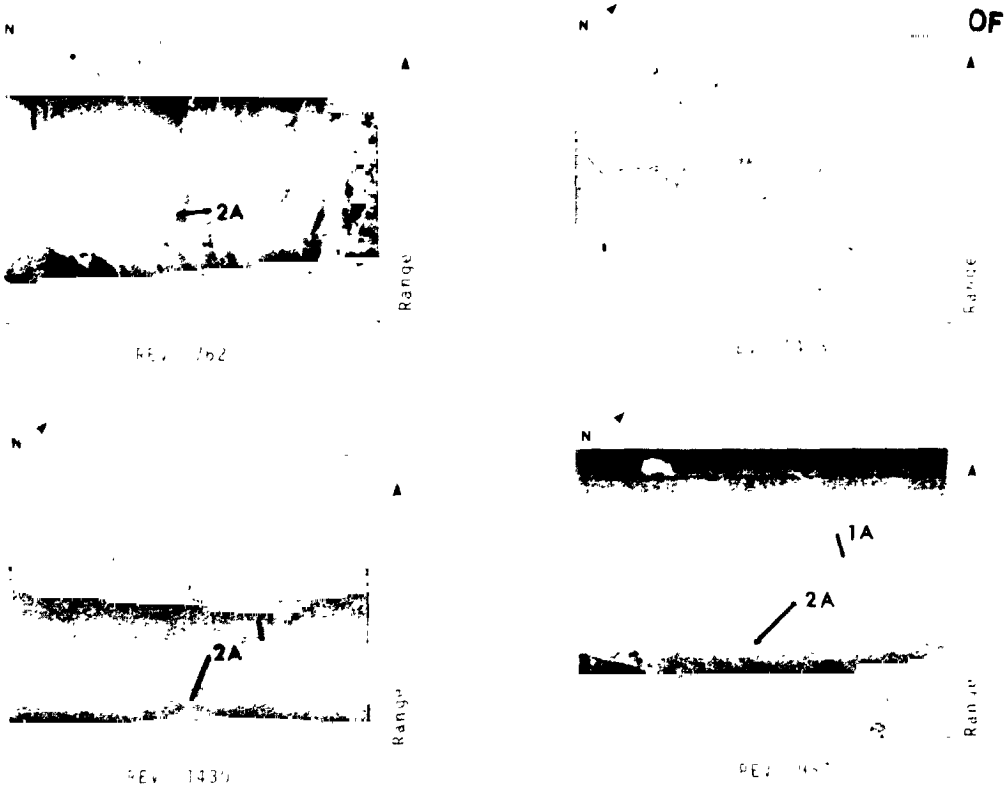

FIGURE 4. SAR IMAGERY OF THE ENGLISH CHANNEL SHOWING THE LOCATIONS OF BACKSCATTER MEASUREMENTS MADE OVER SOUTH FALLS AND SANDETTIE BANKS (Azimuth is Horizontal)

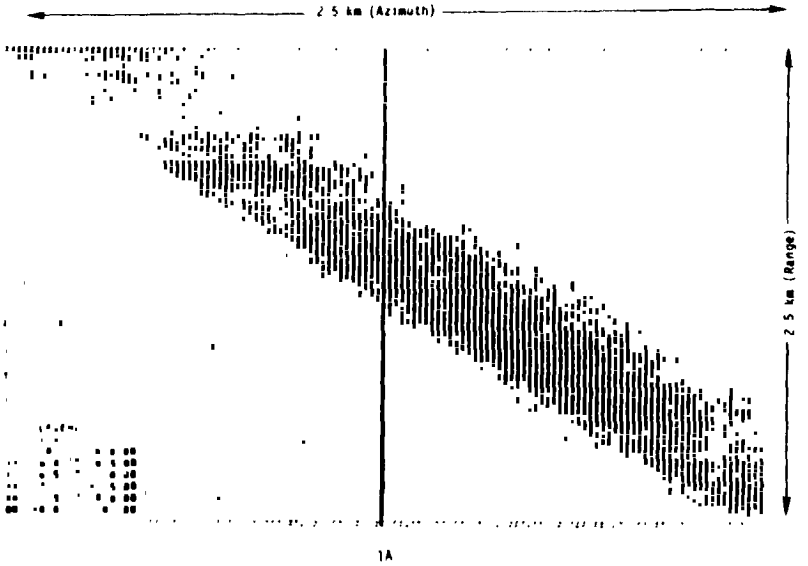

FIGURE 5. M ELED BACKSCATTER MAP FOR REV. 762 SHOWING GOOD VISIBILITY OF SOUTH FALLS

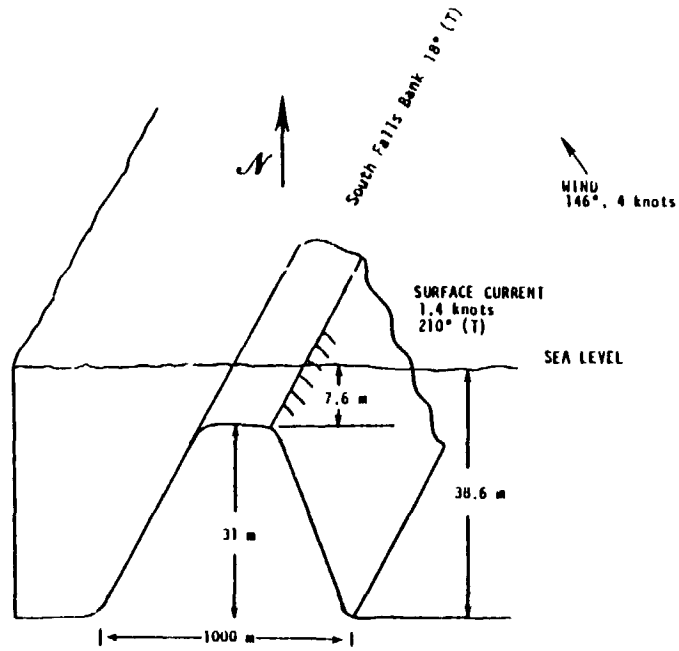

FIGURE 6. IDEALIZED CROSS SECTION OF SOUTH FALLS, SEASAT REVOLUTION 762

TABLE 4
COMPARISON BETWEEN MODELED AND ACTUAL SAR BACKSCATTER VALUES

Revolution	Subsurface Feature	EM Model Results (dB) Min. σ_0	Max. σ_0	$\Delta\sigma_0$	Actual Seasat SAR Backscatter Values (dB) Min. σ_0	Max. σ_0	$\Delta\sigma_0$
762	South Falls	-2.7	1.3	4.0	-2.4	1.4	3.8 (D)
					-2.2	1.1	3.3
957	South Falls	-0.2	0.1	0.3	0.0	0.0	0.0
1430	South Falls	-0.4	0.3	0.7	0.0	0.0	0.0
1473	South Falls	-0.6	0.5	1.1	-1.7	0.9	2.6
762	Transverse Sand Waves	-2.4	1.3	3.7	-2.3	1.6	3.9 (D)
762	Sandettie Sand Bank	0.0	0.0	0.0	-3.1	2.0	5.1 (D)
957	Sandettie Sand Bank	0.0	0.1	0.1	-0.2	0.1	0.3
1430	Sandettie Sand Bank	0.0	0.0	0.0	-0.3	0.3	0.6
1473	Sandettie Sand Bank	-0.5	0.4	0.9	-0.8	1.1	1.9

(D) Indicates Seasat SAR backscatter value was obtained from digital data. Note actual measurements are relative backscatter, they have been normalized to average model value.

less than 0.5 dB. Note that the table gives relative backscatter values, and thus the problem of absolute calibration is avoided. Examination of the South Falls case reveals a model prediction of backscatter variations of 0.3 and 0.7 dB for Revolutions 957 and 1430, respectively. The Seasat images for these revolutions showed very faint or invisible features near South Falls, and the optical measurements yielded no measurable change in radar cross section over the ridge.

For Revolution 1473, the model predicted a backscatter variation of 1.1 dB over South Falls and the empirical measurements showed a variation of about 2.5 dB across the ridge. The image for this revolution shows a clearly identifiable feature corresponding to South Falls, although the feature is less distinct than in Revolution 762. The fact that the measured decrease in the radar return is larger in magnitude than the model result, while the measured increase is about the same, appears to indicate that the actual wind regeneration effect was smaller than that incorporated in the model. It should be noted that there is a fairly wide disparity in measurements of the wind growth rate, and this parameter is not completely understood at the present time (Hughes, 1978).

To further validate the model, the digital SAR data from Revolution 762 was compared in detail with the model results. Figure 7 represents a one-dimensional slice of model results compared with the actual SAR digital backscatter values of the same area. On the figures, the solid lines indicate the radar cross section calculated from the model, while the dotted line is the relative radar cross section obtained from the digitally processed Seasat SAR data. Presented on the figure are comparisons between model and actual values for the South Fall Bank and transverse waves corresponding to Revolution 762 environmental conditions. The comparison between model and actual data is quite good for both South Falls and the transverse waves case. The model and actual SAR backscatter are within 1.0 dB of each other everywhere on the two graphs. The sharp peak in the transverse sand wave case is predicted by the model, and is a result of wind direction with respect to the ridge and the current.

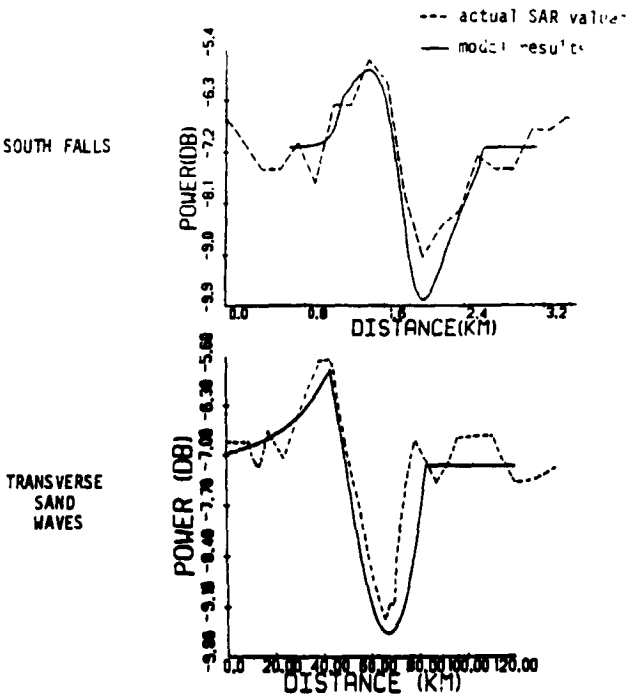

FIGURE 7. MODEL VS. ACUAL BACKSCATTER CROSS SECTION FOR REVOLUTION 762 SOUTH FALLS AND TRANSVERSE SAND WAVES CASE

The hydrodynamic model predicted no change in radar cross section over the Sandettie Sand Bank for the Revolution 762 case, where the bank is aligned in the cross-track direction. The fact that this feature was observed, with approximately a 5 dB change in backscatter, appears to indicate an additional mechanism not incorporated in the model. This additional mechanism will be discussed in the next section. Modeled results over the Sandettie test site for Revolutions 957 and 1473 were in better agreement with actual SAR values (to within 1.0 dB).

In summary, it appears that when the calculated variation in the radar cross section is greater than 1 dB, the feature is visible in the Seasat SAR image. When the calculated variation is less than 1 dB, the feature is very faint or not visible in the image.

5. DISCUSSION OF MODEL RESULTS

The hydrodynamic/electromagnetic model was run for three locations within the English Channel test site. Table 4 summarized the comparison between the modeled and actual backscatter values. As presented earlier, the modeled results compare quite favorably (within 1.5 dB) to the actual Seasat SAR values.

The notable exception to the favorable comparison was the Sandettie Sand Bank test site for Revolution 762. Recall from Figures 1 and 2 that Sandettie Bank, as imaged during Orbit 762, is aligned along the radar line of sight.

The alignment of Sandettie Bank on Revolution 762 is such that the bank's long axis is within a few degrees of the across-track direction of the SAR coordinate system. Using the simplified current model described earlier (Eqs. 2 and 3), the current component (V_y) in the across-track direction is constant for this case. Therefore, the Bragg waves are not influenced by this current, as indicated by Eq. (6), and the model does not predict any change in radar cross section across Sandettie Bank. This is in apparent contradiction to the SAR image, which shows a distinct variation in this region.

The apparent failure of the model for this feature may be due to several reasons, including the following: (1) the simple current model may not be adequate for this case, and there may actually be changes in V_y along the ridge, (2) the fact that the ridge is not smooth, i.e., there are numerous transverse sand waves along the ridge which are actually responsible for the observed image variations, and (3) the radar return is influenced by changes in other surface waves.

The latter possibility is suggested by the fact that there are likely to be large perturbations of waves traveling in a direction other than the across-track direction. The response of the radar to those waves could be due to non-Bragg scattering mechanisms or to non-linear wave-wave interactions which influence the Bragg waves. One possible reason for these non-linear interactions could be the existence of large wave amplitudes occurring due to wave blocking.

Each individual component of the small-scale ocean surface wave structure will be blocked when it encounters an adverse current velocity of magnitude level equal to one-half its phase speed (or equal to the group speed for this wave component). As an example, the Bragg waves for an L-band radar system with Seasat radar geometry will be blocked by a change in the adverse flow rate of 0.36 m/s from the ambient level. For conditions of Sandettie Bank, a change in local water depth of 1.9 m along the crest of the ridge is sufficient to induce blocking of the Bragg wave. This range of depth change is certainly within the realm of possibility for this region of the English Channel. Should the depth undulate along the crest

of the ridge, periodic blocked wave structures should exist in the received radar backscatter signal.

6. SUMMARY AND RECOMMENDATIONS

A hydrodynamic and electromagnetic modeling effort has been undertaken for the purpose of explaining and quantifying Seasat synthetic aperture radar (SAR) backscatter signatures that relate to the bottom topography of the oceans. Large quantities of Seasat SAR imagery have been reviewed revealing the existence of surface expressions of sub-surface features on many passes of imagery. The most vivid of these cases are those surface expressions associated with shoal regions (50 meters and less water depth) east of Nantucket Island and the Southern Bight of the North Sea (English Channel). The English Channel, characterized by shallow, sub-aqueous banks and sand waves, was studied as part of this modeling effort.

The hydrodynamic model developed and utilized within this study embodies the interaction of a tidal current with the bottom features and the interaction of the surface Bragg waves with the current variations. The hydrodynamic model utilizes as inputs environmental data (wind, waves, currents, depth, tides and density stratification) coincident with the SAR data collection and predicts as output the change in the small scale roughness (i.e., Bragg wave amplitude) of the ocean surface.

A SAR reflectivity model for the ocean was also developed as part of this study. A specialized form of the developed SAR electromagnetic model utilized the small scale roughness as produced by the hydrodynamic model along with the Seasat SAR system parameters (frequency, polarization, incident angle and resolution) to generate SAR reflectivity gray maps of images showing varying degrees of bottom features. This specialized SAR model neglected scatterer motion effects and large slope change. It should be noted that neglecting these two factors did not diminish the prediction capability of the model, except possibly in one case in which the bottom feature (ridge) was aligned in the across-track direction.

Four Seasat passes showing various degrees of bottom feature visibility were selected for use in the model verification. The surface expressions were first correlated with depth changes. The modeled results predicted SAR features associated with bottom topography which agreed, at least to a first order, with actual SAR observations. The predictions agreed qualitatively with the observations in the sense that bright and dark bands are observed in the SAR images in the locations predicted by the model. The predictions also agree quantitatively with measurements of the radar cross section to within 1.5 dB, except in the case of a bottom feature (ridge) aligned in the across-track direction. Based on these cases, features appear to be visible in the Seasat SAR imagery if the backscatter variations predicted by the model are larger than 1 dB.

Based upon the results of this investigation, the following conclusions can be made regarding the environmental conditions required for visibility of bottom topographic features in SAR imagery. These conditions may be stated as follows:

1. A tidal current of at least 0.40 m/sec (0.80 Kts) must be present.

2. A wind of at least 1 m/s (2 Kts), but not greater than 7.5 m/s (15 Kts) must be present, with at least some component in the radar range direction.

These conclusions have been reached on the basis of the model as presently developed and as applied to relatively distinctive shallow bottom features in the English Channel. The actual limits on the current and wind may be different for other geographical locations, and could be further refined by more extensive model development and verification.

The problems associated with further development and testing of this model include obtaining adequate sea truth collected concurrently with SAR data. Specifically, actual depth values registered to the SAR images need to be obtained along with the two-dimensional current profile that was present at the time of SAR overflight. Further aircraft and spaceborne SAR programs (i.e., SIR-B and ERS-1) could certainly address this deficiency. From a theoretical standpoint, certain aspects of the model need to be improved to properly simulate all geometries. In particular, wave blocking and perhaps non-linear long-wave/short-wave interaction must be taken into account.

7. ACKNOWLEDGEMENTS

The work reported in this paper was performed at the Environmental Research Institute of Michigan (ERIM) under contract in part to four government agencies. The agencies and the technical monitors include: Office of Naval Research (Mr. Hans Dolezalek), Defense Mapping Agency/Naval Research Laboratory (Dr. James Hammack, and Mr. Peter Mitchell), National Oceanic and Atmospheric Administration (Mr. John W. Sherman, III), and the National Aeronautics and Space Administration (Drs. Lawrence McGoldrick and William Patzert). The contract numbers for these funded research activities are: ONR Contract N00014-81-C-2254, DMA Contract 800-78-C-0060, NRL Contracts N00014-81-C-2254 and N00014-82-C-2308, ONR (NASA) Contract N00014-81-C-0692; and NOAA/NASA Seasat Announcement of Opportunity Contract MO-A01-78-00-4339.

8. REFERENCES

Alpers, W.R. and C.L. Rufenach, The Effect of Orbit Motions on Synthetic Aperture Radar Imagery of Ocean Waves, IEEE Trans. Antennas Propagat., Vol. AP-27, pp. 635-690, 1979.

Alpers, N.R., D.B. Ross, and C.L. Rufenach, On the Detectability of Ocean Surface Waves by Real and Synthetic Aperture Radar, J. Geophys. Res., 86, 6481, 1981.

Caston, G.F., Wreck Marks: Indicators of Net Sand Transport, Marine Geology, Vol. 33, pp. 193-204, 1979.

Harger, R.O., Synthetic Aperture Radar Systems, Academic Press, New York, NY, 240 pp., 1970.

Hughes, B.A., The Effect of Internal Waves on Surface Wind Waves: Part 2, Theoretical Analysis, J. Geophys. Res., 83, pp. 455-465, 1978.

Jain, A., Focusing Effects in Synthetic Aperture Radar Imaging of Ocean Waves, J. Appl. Phys., Vol. 15, pp. 323-333, 1978.

Kasischke, E.S., R.A. Shuchman, D.R. Lyzenga, and G.A. Meadows, Detection of Bottom Features on Seasat Synthetic Aperture Radar Imagery, Photogrammetric Engineering and Remote Sensing, Vol. 49, No. 9, pp. 1341-1353, 1983.

Kasischke, E.S., R.A. Shuchman, J.D. Lyden, G.A. Meadows, D.R. Lyzenga, and E.M. Jurecki, The Use of Satellite and Aircraft SAR to Detect and Chart Hazards to Navigation, ERIM Final Report No. 163000-1-F, Ann Arbor, MI (in press), 1983a.

Kenyon, N.H., Bedforms of Shelf Seas Viewed with Seasat Synthetic Aperture Radar, in Advances in Holographic Surveying, ed. by M.J. Wright, Society for Underwater Technology, London, pp. 69-73, 1981.

Kenyon, N.H., R.H. Belderson, A.H. Stride, and M.A. Johnson, Offshore Tidal Sand Boules as Indicators of Net Sand Transport and as Potential Deposits, in Holocene Marine Sedimentation in the North Sea Basin, Selected Papers from the IAS Meeting, Texel, Netherlands, ed. by S.D. Nio, R.T.E. Schuttenhelm and T.C.E. Van Weering, IAS Spec. Pub. 5., 1979.

Lyzenga, D.R. and R.A. Shuchman, Analysis of Scatterer Motion Effects in MARSEN X-Band SAR Imagery, J. of Geophys. Res., Vol. 88, No. C11, 1983.

Lyzenga, D.R., A.L. Maffett, and R.A. Shuchman, The Contribution of Wedge Scattering to the Radar Cross Section of the Ocean Surface, IEEE Trans. on Geoscience and Remote Sensing, Vol. GE-21, No. 4, pp. 502-204, 1983.

Phillips, O.M., The Dynamics of the Upper Ocean, Second Ed., Cambridge Univ. Press, 1977.

Phillips, O.M., The Structure of Short Gravity Waves on the Ocean Surface, in Spaceborne Synthetic Aperture Radar for Oceanography, ed. by R.C. Beal, P.S. DeLeonibus, and I. Katz, Johns Hopkins Univ. Press, Baltimore, MD, pp. 24-31, 1981.

Shuchman, R.A., A.L. Maffett, and A. Klooster, Static and Dynamic Modeling of a SAR Imaged Ocean Secne, IEEE J. Oceanic Eng., Vol. OE-6, 1981.

Shuchman, R.A., Quantification of SAR Signature of Shallow Water Ocean Topography, University of Michigan PhD Dissertation, Ann Arbor, Michigan, 130 pp., 1982.

Vesecky, J.F. and R.H. Stewart, The Observation of Ocean Surface Phenomenon Using Imagery from the Seasat Synthetic Aperture Radar - An Assessment, J. Geophys. Res., 87, pp. 3397-3430, 1982.

Wright, J.W. Backscattering from Capillary Waves with Application to Sea Clutter, IEEE Trans. Antenna Propagat., Vol. AP-14, pp. 749-754, 1966.